Velocity Analysis of Thermionic Emission from Single-Crystal Tungsten*†

ANDREW R. HUTSON‡
Research Laboratory of Electronics, Massachusetts Institute of Technology, Cambridge, Massachusetts
(Received January 13, 1955)

A 180° magnetic velocity analyzer tube has been used to observe the energy distributions of the thermionic emission from various crystallographic directions of a single-crystal tungsten filament. The distributions were the same in all of the directions and were not Maxwellian. An energy-dependent reflection coefficient for the tungsten surface, previously proposed by Nottingham, is capable of explaining the shape of the distributions quite well. The tube permitted measurements of the differences between the true work functions of the various directions. The changes of true work functions with temperature between 1700°K and 2000°K were also measured for all directions except the (110). The non-Maxwellian character of the energy distributions and the temperature variations of the work functions can largely explain the discrepancy between the emission constant, $A=120$, of Richardson's equation and the Richardson-plot emission constants obtained for the various directions of a tungsten crystal by Nichols and by Smith.

I. INTRODUCTION

AT the present time, knowledge of the phenomenon of thermionic emission is still incomplete. Thermodynamics and the Fermi-Dirac statistics yield the well-known Richardson equation, $j=AT^2(1-\bar{R})\exp(-e\phi/kT)$, when applied to an electron gas in equilibrium with a metal of work function ϕ at a temperature T. The emission constant, A, is made up of well-known physical constants and is 120 amperes/cm^2 deg^2, and $\bar{R}$ is an average reflection coefficient for the metal surface. However, this equation, without the factor $(1-\bar{R})$, is usually applied empirically to the situation in which saturation current is being drawn from the metal surface. A Richardson plot of the variation of emission current with temperature is used to obtain empirical values of the work function and emission constant. These values may differ from the true work function and the A of 120 because of "patchiness" of the surface, temperature variation of the true work function, and reflection at the metal surface. The review article by Herring and Nichols[1] treats both the thermodynamic aspects of the Richardson equation and these difficulties in its application.

Nichols[2] was the first to make quantitative measurements of the emission from a single crystal of tungsten in the crystallographic directions of maximum and minimum emission. He obtained Richardson plot values for the work functions and emission constants in the various directions. Smith[3] has recently repeated this experiment with some refinements in technique, and his results are in substantial agreement with those of Nichols. The empirical emission "A" constants obtained in the different directions differ from one another, and with the exception of the (112) direction they are all less than 120. From the results of this experiment, one cannot distinguish between the effects of patchiness, temperature variation of the work function, and reflection.

Both patchiness and reflection, if it is energy-dependent, would result in an anomalous energy distribution of the emitted electrons. If there were no patchiness or reflection, one should observe an energy distribution characteristic of the particle current of a Maxwell-Boltzmann gas, since the density of the electron gas in equilibrium with the metal is low enough for the Fermi-Dirac distribution to be well represented by the classical distribution. (The principle of detailed balance requires that the energy distribution of the particle current from the metal surface be the same as that of the particle current in the gas provided that there is no reflection at the metal surface.) The only observations of energy distribution have been made in terms of retarding-potential data in which one obtains the integral under the energy distribution curve from a variable lower limit to infinity instead of the curve itself. Nottingham[4] found that his careful retarding-potential measurements on tungsten and thoriated tungsten could be best represented by an empirical reflection coefficient, which was an exponential function of the energy associated with motion perpendicular to the surface. The fact that all of Nottingham's retarding-potential curves for tungsten and thoriated tungsten in all states of activation could be represented accurately by a single reflection coefficient is significant, in that it tends to support the view that one is dealing with a fundamental reflection effect rather than patchiness.

A previous measurement of the temperature coefficient of the work function of polycrystalline tungsten at thermionic temperatures has been made by Krüger and Stabenow.[5] They obtained an average value of $+6\times10^{-5}$

* This work was supported in part by the Signal Corps; the Office of Scientific Research, Air Research and Development Command; and the Office of Naval Research.

† This paper is based on a thesis submitted by Andrew R. Hutson in partial fulfillment of the requirements for the degree of Doctor of Philosophy in the Department of Physics of the Massachusetts Institute of Technology.

‡ Now at Bell Telephone Laboratories, Murray Hill, New Jersey.

[1] C. Herring and M. H. Nichols, Revs. Modern Phys. **21**, 185 (1949).

[2] Myron H. Nichols, Phys. Rev. **57**, 297 (1940).

[3] George F. Smith, Phys. Rev. **94**, 295 (1954).

[4] W. B. Nottingham, Phys. Rev. **49**, 78 (1936).

[5] F. Krüger and G. Stabenow, Ann. Physik **22**, 713 (1935).

Stabenow.[5] They obtained an average value of $+6\times10^{-5}$ ev/deg in the temperature range 2100°K to 2700°K by a calorimetric method. They claimed an accuracy of 20–30 percent for this result, however, their vacuum conditions were poor by modern standards. Langmuir[6] and Potter[7] have obtained values for the temperature coefficient of polycrystalline tungsten between room temperature and 1000°K. Their results are in disagreement, being of opposite sign, and in any case an extrapolation to thermionic temperatures would not be warranted.

In the present experiment, magnetic velocity analysis of the thermionic emission from a single-crystal tungsten filament has yielded: (1) the energy distributions of the emission in the various crystal directions, (2) the temperature coefficients of the work functions in the various directions, and (3) the actual differences in work function between the different directions at thermionic temperatures. The results of the first two measurements can satisfactorily explain the A values obtained by Nichols and by Smith. The third measurement serves as a check on the self-consistency of the interpretation.

II. FILAMENT PREPARATION

The growth of single crystals in G.E. "218" tungsten wire (of the pre-World War II variety) occupying the entire cross section and extending over several centimeters of length is now a well-known art. Robinson[8] has shown that one need only hold the temperature of the wire in the recrystallization range (about 2000°K) for a few hours to obtain large single crystals. There appears to be an optimum temperature for the process, above which many small crystals are produced because of the increased rate of formation of seed crystals, and below which the linear growth from a given seed crystal becomes impractically slow. The crystals grow with a face diagonal (110) direction, in the axis of the wire as a result of strains imparted to the wire in the drawing process. The crystal faces which can then be exposed on the surface must have as their normals the directions (*hhk*). Martin's[9] study of the emission from a single-crystal tungsten sphere showed that the principal maxima and minima of emission occurred on just these planes, though recent field-emission work[10] has also included a minor maximum in the (310) direction.

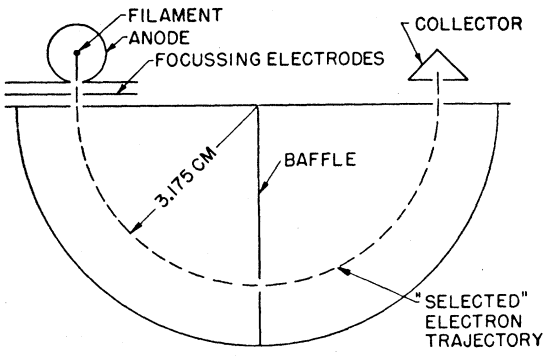

FIG. 1. Cross section of the analyzer tube.

The "dopes" which are added to the tungsten in fabrication to catalyze this growth of large crystals are largely driven out in the sintering and swaging processes. Nichols[11] gives the results of spectroscopic analyses of doped and undoped tungsten as well as their average Richardson plot emission constants and work-functions. He shows that the lower values of A^{**} and ϕ^{**} for the doped wire are merely due to the higher degree of preferred orientation, and that the crystals in "218" wire should be characteristic of pure tungsten.

As it comes from the manufacturer, the surface of the tungsten wire contains many deep longitudinal die scratches and therefore must be ground and polished smooth since accurate knowledge of the applied field demands a smooth surface. The grinding and polishing was carried out on a specially constructed wire polisher[12] which rotates the wire between a pair of laps, coated with abrasive, that traverse the length of the wire on a carriage driven by a lead screw.

The filament used for the present experiment was ground and polished from an initial diameter of 0.003 inch to about 0.002 inch as read on a micrometer caliper. After polishing, the wire appeared to have a mirror surface with just the faintest indication of abrasive scratch under observation with a 400× optical microscope. Johnson[13] has shown that these light scratches disappear during subsequent ac heating, and his observation has been verified for a number of filaments.

The diameter of the filament was measured by an interferometric technique with the 5461 A mercury line. The average of several readings along its length yielded a value of 5.16×10^{-3} cm.

The filament was given its recrystallization heat treatment in a cylindrical electron projection tube[14] in which the pattern of the intensity of thermionic emission may be observed directly. In this manner, the growth and quality of the large single crystals growing in the filament were easily monitored. Alternating current was used for filament heating in order to avoid dc etch, a peculiar type of surface roughening believed to be due to the effect of a longitudinal electric field upon the surface migration of the tungsten atoms.[15]

One interesting peculiarity was observed in the

[6] David B. Langmuir, Phys. Rev. **49**, 428 (1936).
[7] James G. Potter, Phys. Rev. **58**, 623 (1940).
[8] C. S. Robinson, Jr., J. Appl. Phys. **13**, 647 (1942).
[9] Stuart T. Martin, Phys. Rev. **56**, 947 (1939).
[10] M. K. Wilkinson, J. Appl. Phys. **24**, 1203 (1953).
[11] M. H. Nichols, Phys. Rev. **78**, 158 (1950).
[12] Johnson, White, and Nelson, Rev. Sci. Instr. **9**, 253 (1938).
[13] R. P. Johnson, Phys. Rev. **56**, 947 (1939).
[14] R. P. Johnson and W. Shockley, Phys. Rev. **49**, 436 (1936).
[15] R. P. Johnson, Phys. Rev. **54**, 459 (1938); R. W. Schmidt, Z. Physik **120**, 69 (1943); D. B. Langmuir, Phys. Rev. **89**, 911(A) (1953).

projection-tube patterns of all of the recrystallized filaments. When the filament temperature was held at 2000°K or lower, the (100) direction appeared as a narrow minimum between two broad (116) maxima, in agreement with previous observations. However, at a filament temperature of 2300°K, the (100) direction appeared as a narrow maximum separated from the (116) maxima by narrow minima. The explanation of this effect is found in the measurements of the temperature variations of the work functions.

III. VELOCITY ANALYZER TUBE

The principal elements of the velocity analyzer tube are shown in cross section in Fig. 1. The single-crystal filament was located coaxially within the cylindrical anode, and was supported in such a manner that it could be rotated about this common axis. Electrons emitted by the filament were accelerated in the radial direction by a positive potential applied to the anode. Those originating from a narrow sector of the filament passed through a slit in the anode and were focused into the entrance slit of the 180° analyzer chamber. The analyzer was a semicircular tantalum box whose faceplate (the diameter of the semicircle) contained the entrance and exit slits which were each 0.026 cm wide and 1.0 cm long. The analyzer chamber was partitioned by a baffle containing a slit of width 0.2 cm. An externally imposed uniform magnetic field, perpendicular to the plane of Fig. 1, caused the electrons to move in circular paths so that those electrons with precisely the right kinetic energy of motion in the plane of the diagram traversed all of the slits and were recorded as collector current.

The focusing electrodes modified the electric fields between the anode slit and analyzer entrance slit in a manner such that this region acted as a doubly convergent lens. This design feature resulted from the conflicting requirements of high angular resolution for the anode slit and sufficient resolution in energy within the analyzer. The anode slit, of width 0.026 cm, defined an angular sector of about three degrees in the one-centimeter diameter anode. However, unless there was a large radial accelerating field at the filament, there would have been a considerable number of electrons originating on either side of this three-degree sector which would have been able to pass through the anode slit by virtue of their initial tangential velocities. Numerical integration of electron trajectories within the anode indicated that an anode potential of about 1000 volts (radial field at the filament $\approx$75 000 volts/cm) would yield satisfactory angular resolution even in the crystallographic directions of lowest emission. This radial field is also much larger than the fields resulting from the differences of work function around the single-crystal filament.

The resolution in energy of this type of analyzer, $\Delta V/V$, is the ratio of slit width to analyzer radius which was 1/125. Thus, to obtain a "slice" of the energy distribution only a few hundredths of an electron volt wide, the electrons had to proceed through the analyzer with an energy of only a few electron volts. For most of the operation of the tube, the electrons were retarded from about 1000 ev to about 3 ev between the anode slit and the analyzer entrance slit ($\Delta V=0.024$ v).

The action of the focusing electrodes upon the ribbon-like beam in the region between the anode and the analyzer is shown in an enlarged cross section in Fig. 2. If the anode slit and analyzer slit had been merely placed face-to-face without the focusing electrodes, the beam would have been divergent in the retarding field between the slits so that only a small fraction of the beam would have entered the analyzer. Also, the analyzer slit itself would have acted as an extremely short focal-length lens so that those electrons which did enter the analyzer would be fanned out and only a few would have been able to pass through the angle-limiting slit in the baffle.

The lens properties of this arrangement of slits were investigated on paper before the tube was finally designed. Solutions of LaPlace's equation in the region shown in Fig. 2 were obtained for a variety of focusing slit potentials by tracing the equipotentials on a large sheet of conducting paper[16] upon which the electrodes had been painted with silver, printed-circuit paint. The paraxial ray equation was integrated point-by-point making use of the values of the potential and the radius of curvature of the equipotentials at the lens axis. After the desired trajectory had been "bracketed" by trajectories obtained with various values of focusing voltage, it was concluded that the optimum focusing potential could best be obtained experimentally.

The structure of the analyzer tube is illustrated in Fig. 3 in which a number of the design features are apparent. With the exception of the collector, all of

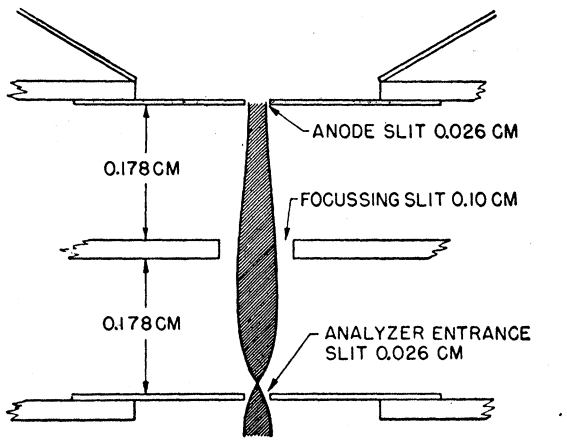

FIG. 2. Enlarged cross section of region between anode and analyzer. The electron trajectories lie within the shaded area.

[16] Manufactured for recording purposes by the Western Union Company under the trade name "Tele-Deltos."

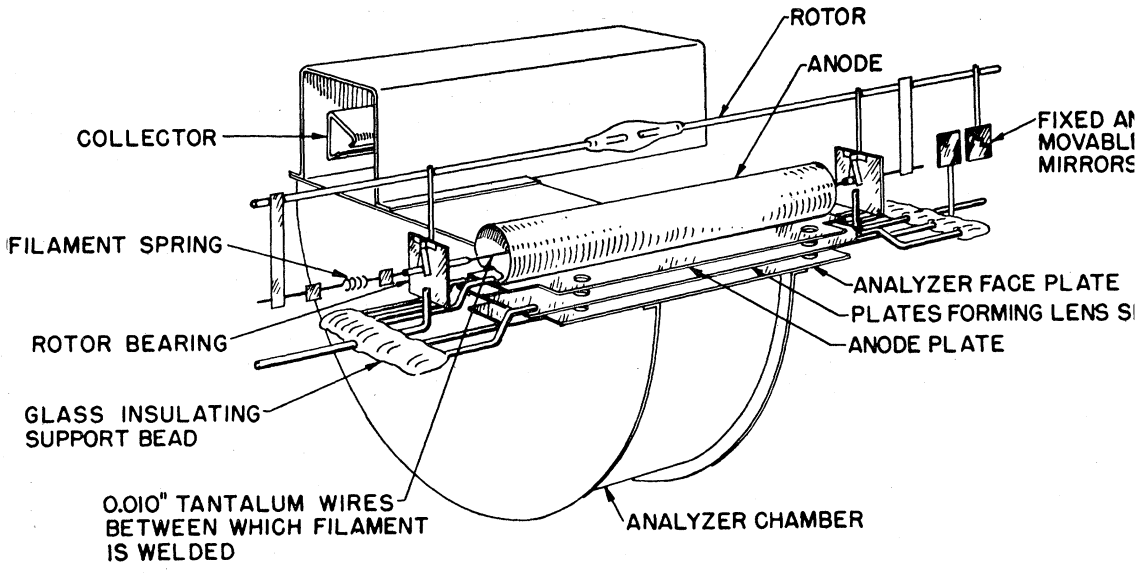

FIG. 3. Illustration of the analyzer structure.

the elements of the structure were mechanically supported by the analyzer face-plate. The face-plate was fabricated from accurately flat 0.020-inch tantalum sheet, and in order that the entrance and exit slits would not appear to be "corridors" they were sawed in a 0.003-inch tantalum sheet which had been welded over rectangular cut-outs in the face-plate. The same technique was used for the anode slit in the 0.010-inch tantalum anode plate. The anode itself was a cylinder, 1.0 cm in diameter, formed from 0.003-inch tantalum sheet. It contained a cut-out, larger than the slit in the anode plate, which fitted over the anode slit when the cylinder was welded tangent to the plate. The lens, or focusing slit, consisted of a gap between two coplanar, insulated 0.010-inch tantalum plates. Insulation of the two sides of the focusing slit allowed the application of a transverse electric field in the lens which could be used to compensate for small errors in the alignment of the slit and filament. All of the slits were sawed on a milling machine. After pre-outgassing the various parts, final assembly of the analyzer, anode, focusing electrodes, and the tantalum plates containing the holes for the rotor shafts was accomplished by flowing glass over the prebeaded tungsten support rods. The alignment holes which can be seen in Fig. 3 were used to hold the parts rigidly in a carefully machined jig (machining tolerances ± 0.0005 inch) during this operation. The advantage of this method of final assembly is that the structure is strain-free after removing the jig, thus all of the slits and the axis of rotation of the filament remained accurately parallel.

The 6-cm length of 0.002-inch recrystallized filament, containing the large single crystal was held on the axis of rotation of the rotor by tantalum wires which passed through guide holes accurately drilled along the axes of the rotor shafts. A tungsten helical spring tained the proper tension in the filament.[17]

The structure of Fig. 3 was supported with th ment axis vertical by a single re-entrant press in inch diameter pyrex envelope. The collector wa ported independently by its own shielded re-e press. In order to rotate the filament, the entire tu tipped so that the rotor would swing under the inf of gravity. (Rotation schemes involving a perm magnet within the tube could not be used beca possible distortion of the analyzing field.)

The evacuation schedule of the tube, involvi peated cycles of baking and outgassing of the stru conformed with modern high-vacuum techniq Bayard-Alpert ionization gauge of our own d was attached to a sidearm of the main envelop sealed off with the tube. Immediately after se the gauge recorded a pressure of 9×10^{-10} mm slowly rose to 1.5×10^{-9} mm, due largely to the di of atmospheric helium through the Pyrex wall gauge remained in continuous operation after se and the pressure remained at 1.5×10^{-9} mm vacuum conditions in the tube proved satisfacto the performance of the experiment. No change total emission of the filament was ever observed. was only one observable change in the analyzer function. It occurred when a measurement was attempted at a filament temperature of 2100° an anode potential of 1000 v. Enough gas was from the anode by electron bombardment to ra pressure in the tube to 4×10^{-9} mm. Subsequent

[17] K. B. Blodgett and I. Langmuir, Rev. Sci. Instr. **5**, 321
[18] R. T. Bayard and D. Alpert, Rev. Sci. Instr. **21**, 571
Research Laboratory of Electronics, Massachusetts Inst Technology, Quarterly Progress Report, Jan. 15, 195 (unpublished).

operation of the ionization gauge served to reduce the pressure once again to 1.5×10^{-9} mm, and no further changes in the analyzer work function were observed.

IV. ELECTRICAL CIRCUITS

A block diagram of the circuit is shown in Fig. 4. The filament was pulse-heated by conduction. Each pulse provided a positive bias voltage across R_b so that electrons could only reach the analyzer when there was no potential drop along the filament due to heating current. The pulse-heater, utilizing a pair of *FG*–67 mercury thyratrons in an inverter circuit, was devised by Nottingham, and has previously been described by him.[19] The temperature of the filament was monitored during pulse-heating by a photoelectric ammeter consisting of a series-connected auxiliary filament which illuminated a phototube whose output was measured by a null method with an *FP*–54 electrometer circuit. Calibration of the photoammeter was accomplished by heating the filament by direct current measured with a 1-ohm standard resistor and a Leeds and Northrup type-*K* potentiometer. The dc heating current corresponding to the desired operating temperature was obtained from the Forsythe-Watson tables[20] of resistivity and emissivity of tungsten and the interferometrically determined diameter of the filament. With the aid of some feedback and the continuous operation of the photoammeter, changes of emission due to changes of filament temperature could be held to less than 1 percent. The correction to the temperature at the center of the filament due to the cooling of its ends was negligible. During the course of the experiment, the filament was operated at 2000°K on pulse-heating for long periods of time. In order to avoid dc etch, the direction of flow of heating current was reversed every ten minutes, and the filament was heated to 2400°K on 60-cycle ac every two or three hours of operation.

The filament bias, which served as the variable in taking energy distributions, was supplied by storage batteries and measured with the type-*K* potentiometer. The anode and lens supplies were electronically regulated, and the anode potential was potentiometered. A Compton quadrant electrometer was used as a null indicator to measure the collector current.

The analyzing magnetic field was produced by a large pair of Helmholtz coils. Since the field necessary for analysis was only a few gauss, the earth's magnetic field was canceled in the region of the analyzer to better than 1 percent by a second pair of Helmholtz coils. The current in each set of coils was obtained from storage batteries and could be potentiometered. An oscilloscope with a high-gain vertical amplifier was connected across the Helmholtz coils in order to detect

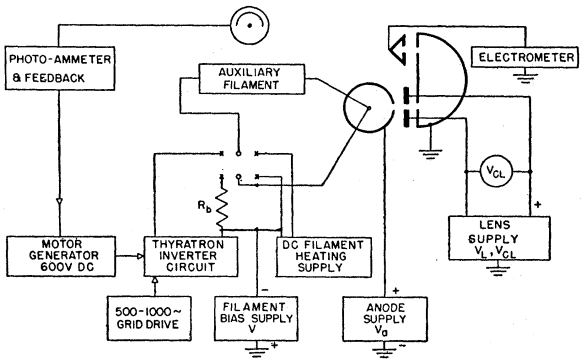

FIG. 4. Block diagram of the circuits used with the analyzer tube.

the presence of any stray, time-varying magnetic fields. No fields were found to have sufficient magnitude to lower the analyzer resolution.

The alignment of the tube in the magnetic field was checked by measuring the slope of a plot of the filament bias, V, necessary to observe either the peak or a half-maximum current point of the thermal energy distribution from a single direction as a function of the square of the Helmholtz coil current, I. This slope is a function of only the dimensions of the Helmholtz coils, the analyzer radius, and e/m for an electron. The analyzer radius calculated from the measured slopes agreed with the designed radius to within one-half the entrance slit-width. When a half-maximum current point was taken as the reference point on the distribution, least-squares analyses of the V *vs* I^2 data indicated a slight curvature which could be ascribed to loss of resolution in the analyzer with increasing electron energy within the analyzer.

V. ENERGY DISTRIBUTIONS AND WORK-FUNCTION DIFFERENCES

The energy distributions of the electrons as obtained in this experiment are expressed in terms of a variable which we have chosen to call V_p. Thus, eV_p is the kinetic energy (expressed in electron volts) associated with two components of the electron's momentum as it crosses the image barrier: p_x, the momentum perpendicular to the filament surface, and p_y, the tangential component perpendicular to the magnetic field. The other component of momentum, p_z, remains unaffected by any field in the tube and need not be considered. The kinetic energy of the electron within the analyzer associated with its motion in the plane perpendicular to the magnetic field is then eV_p plus the difference in potential energy between the point of emission (at the top of the image barrier) and the inside of the analyzer chamber. This change of potential is $(V+\phi_f-\phi_a)$, where $-V$ is the filament bias potential, ϕ_f is the true work function of that part of the crystal from which the electron was emitted, and ϕ_a is the average work function of the inside of the analyzer chamber. The condition that must be satisfied

[19] W. B. Nottingham, Phys. Rev. **41**, 793 (1932); W. B. Nottingham, Phys. Rev. **55**, 203 (1939).
[20] W. E. Forsythe and E. M. Watson, J. Opt. Soc. Am. **24**, 114 (1934).

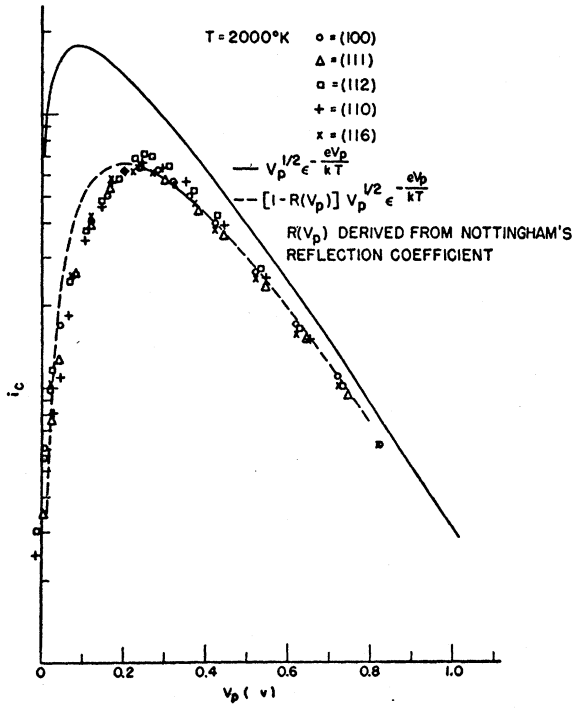

FIG. 5. Superposition of the energy distributions obtained from the directions of maximum and minimum emission with an anode potential of 1000 v. The Maxwellian distribution, and the Maxwellian distribution modified by Nottingham's reflection coefficient are shown for comparison.

in order that the electron may reach the collector is then

$$V+\phi_f-\phi_a+V_p=\tfrac{1}{2}(e/m)B^2R_0^2, \qquad (1)$$

where B is the magnetic field and R_0 is the analyzer radius.

The energy distribution of the electrons in the variable V_p is obtained directly by plotting collector current, i_c, as a function of filament bias, V, at constant magnetic field. This method of taking the distributions has two desirable features: the "slice" of the energy distribution remains the same in scanning the distribution, and the only field change within the tube is a change of 0.1 percent in the radial accelerating field within the anode.

The focusing fields between the anode and analyzer do not differentiate between electrons whose initial energy was largely associated with p_x or with p_y upon emission. The reason for this may be seen in the expression for the radial component of momentum at the anode slit,

$$p_r^2=2meV_a+p_x^2+p_y^2[1-(r_0/r_1)^2], \qquad (2)$$

and the very small ratio of filament radius to anode radius, $r_0/r_1=0.005$. The lack of dependence of the energy distribution shapes upon the exact conditions of focussing was experimentally verified by defocussing the lens. The beam cross-over (see Fig. 2) was moved backwards and fowards and from side to side with no change in distribution shape, although collector currents were drastically reduced.

A superposition of the experimental energy distributions at 2000°K for the important crystallographic directions is shown in Fig. 5. The data identified as (116) were actually taken in a direction between the (114) and (116) where the emission has a maximum, which therefore corresponds with the direction for which Nichols[2] and Smith[3] made Richardson plots. Note that in Fig. 5 the collector current is plotted on a logarithmic scale, allowing the distributions to be superposed without the use of scale factors. The horizontal shifts along the V axis which are necessary in order to superpose the distributions taken in different crystallographic directions yield the differences between the work functions in these directions [see Eq. (1)]. The work-function differences obtained from the distributions of Fig. 5 are shown in Table I. These are true work-function differences at 2000°K and should not be confused with the differences between Richardson plot work functions. The very high work function in the (110) direction seems to bear out, at least qualitatively, field emission work[21] and the estimates made by Smith.[3]

The shape of the energy distribution is of particular interest. In Fig. 5 one can see that the energy distribu-

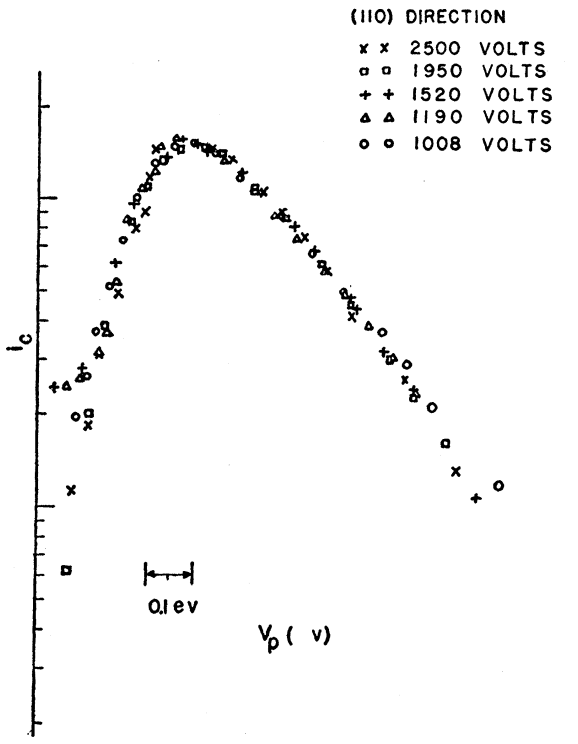

FIG. 6. Superposition of energy distributions obtained at 2000°K in the (110) direction at different anode potentials.

[21] M. Drechsler and E. W. Müller, Z. Physik **134**, 208 (1953); Dyke, Trolan, Dolan, and Grundhauser, J. Appl. Phys. **25**, 106 (1954).

tions from the different directions are identical to within experimental accuracy. The Maxwellian distribution, $V_p^{\frac{1}{2}}\exp(-eV_p/kT)$, lies above the experimental points for low energies indicating a deficiency of slow electrons for "saturation" emission. Such a deficiency of slow electrons may be described by an energy-dependent reflection coefficient for the emitting surface. (In fitting experimental distributions to the Maxwellian distribution, the experimental points on the high-energy side of the distribution are assumed to approach the Maxwellian curve asymptotically, and $V_p=0$ is determined as the point on the low side of the distribution where the slope is characteristic of the resolution of the analyzer. This procedure amounts to finding the smallest possible reflection coefficient which will explain the data.) Nottingham[4] observed a similar dearth of slow electrons in carefully taken retarding-potential data. He developed a reflection coefficient which is an exponential function of the momentum in the direction perpendicular to the surface at the top of the image barrier, $R(p_x)=\exp(-p_x^2/2me\omega)$, in which he determined the parameter $\omega=0.191$ ev from his data. In order to apply this reflection coefficient to distributions in V_p it is necessary to convert $R(p_x)$ to $R(V_p)$. This can be accomplished by multiplying the Maxwellian distribution, written in terms of $p_r=(p_x^2+p_y^2)^{\frac{1}{2}}$ and $\theta=\tan^{-1}(p_y/p_x)$, by the transmission coefficient $[1-\exp(-p_r^2\cos^2\theta/2me\omega)]$, and integrating over θ. The result is

$$R(V_p)=x^{-1}\exp(-x^2)\int_0^x \exp(y^2)dy=x^{-1}F(x), \quad (3)$$

where $x=(V_p/\omega)^{\frac{1}{2}}$, and $F(x)$ has been tabulated by Miller and Gordon[22] for values of the argument between 0 and 12.

The dashed curve in Fig. 5 is the Maxwellian distribution modified by this reflection coefficient using the value of ω determined by Nottingham. The fit to the experimental points is remarkably close.

These distributions were obtained with a magnetic field corresponding to an electron energy within the analyzer of 3 ev. Distributions obtained at 5 ev in the analyzer were similar, indicating that the distribution shape did not depend upon analyzer resolution as long as the resolution was high.

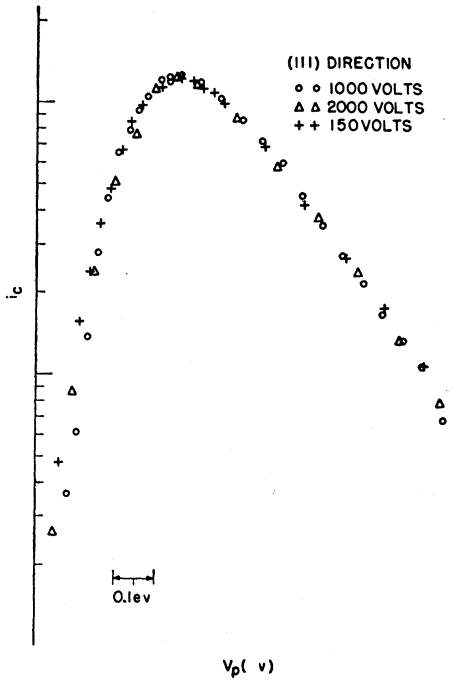

FIG. 7. Superposition of energy distributions obtained at 2000°K in the (111) direction at different anode potentials.

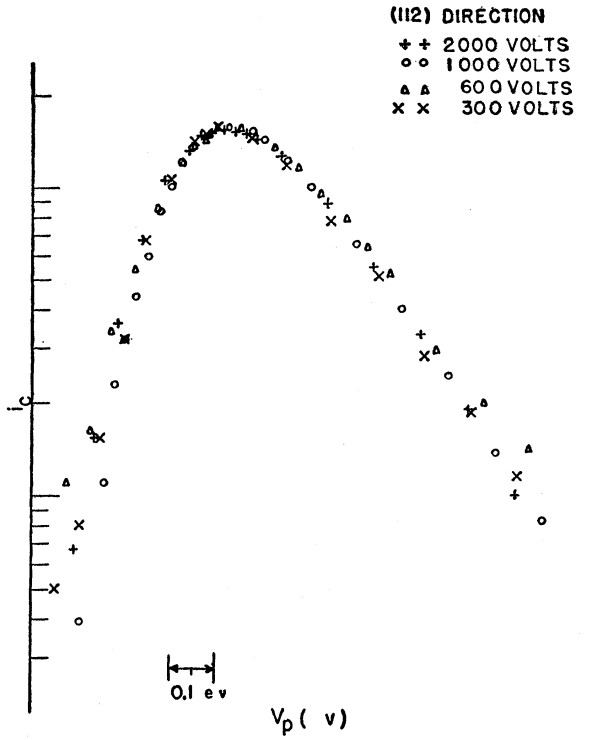

FIG. 8. Superposition of energy distributions obtained at 2000°K in the (112) direction at different anode potentials.

VI. FIELD EFFECTS

Energy distribution data were taken at a variety of different anode potentials in the (110), (111), and (112) directions in attempts to observe any dependence of the reflection effect on applied field. Figures 6–8 are superpositions of the data taken in these three directions. Although the data in the (110) direction and the energy distribution for $V_a=600$ v in the (112) direction

[22] W. Larsh Miller and A. R. Gordon, J. Phys. Chem. 35, 2785 (1931), see Table XXVIII.

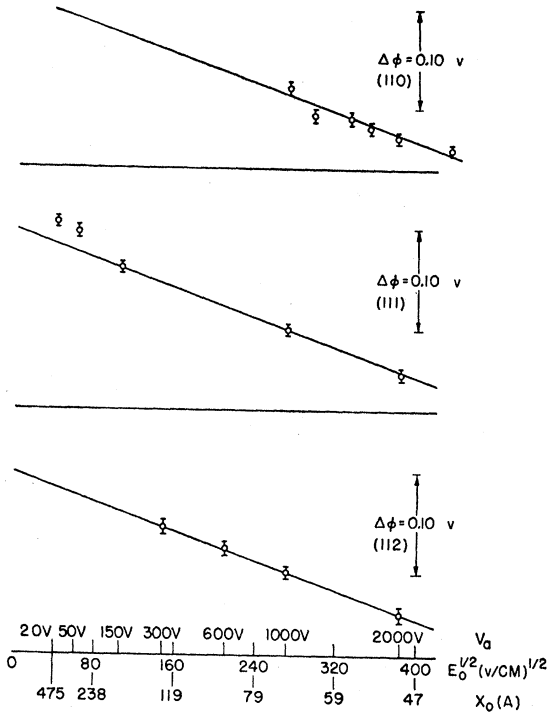

FIG. 9. The change of work function with applied field (Schottky effect) as obtained from the shifts along the voltage axis necessary to superpose the distributions of Figs. 6–8. The solid lines are plotted with the theoretical slope.

show the effects of a small background current, there appears to be *no* significant variation in the shape of the energy distribution with applied field. The changes in reflection coefficient which are responsible for the periodic deviations from Schottky plots are probably too small to be observed in these distributions which are characterized by a reflection coefficient which is appreciable over tenths of volts of energy.

By plotting the change in work function, as obtained from the shifts along the voltage axis required for superposition of the distributions, as a function of the square root of the applied field in Fig. 9, "direct" Schottky plots are obtained. The lines have the theoretical slope, the field being determined from the anode potential, anode radius, and the interferometrically determined filament radius. The probable errors indicated on the experimental points are those associated with uncertainty in the position of "best match" of two distributions. This uncertainty of ± 0.005 v in work-function difference measurement is better than one might assume on the basis of the resolution, $\Delta V/V$, because the transmission of the analyzer is a peaked function of electron energy.

TABLE I. True work function differences (in volts) between crystal faces of tungsten at 2000°K.

$(\varphi_{116}-\varphi_{111})$	-0.01
$(\varphi_{100}-\varphi_{111})$	$+0.02$
$(\varphi_{112}-\varphi_{111})$	$+0.12$
$(\varphi_{110}-\varphi_{111})$	$+0.71$

The two points which lie above the theoretical line in the (111) direction represent distributions taken at extremely low anode voltage where there has undoubtedly been a loss of resolution in azimuth within the anode. As might be expected, since the (111) direction is one of minimum work function, these two points indicate that the work function appears to rise as electrons from higher work-function regions neighboring the (111) direction become part of the measured current. Sizable contributions from neighboring directions of lower work function were apparent in the (110) direction for $V_a<1000$ v, and therefore no measurements at lower fields were attempted in this direction.

VII. TEMPERATURE DEPENDENCE OF WORK FUNCTIONS

The rates of change of work function with temperature in the various directions were derived from shifts along the V axis between distributions for the same direction at different temperatures. The change of distribution shape with temperature required the following technique:

Energy distributions were taken at 2000°K and 1700°K in all of the important directions except the (110) by varying V at constant magnetic field. Logarithmic plots of the 2000°K distributions were then fitted to the Maxwellian distribution, $V_p^{\frac{1}{2}}\exp(-eV_p/2000k)$, in such a manner as to yield an experimental reflection coefficient, $R(V_p)$. The position of $V_p=0$ of the Maxwellian distribution was marked on the V axis of the experimental distribution. The 2000°K experimental points as fitted to the Maxwellian distributions are shown in Figs. 10(a)–(d). By applying the experimental $R(V_p)$'s to $V_p^{\frac{1}{2}}\exp(-eV_p/1700k)$ one obtains the distributions to be expected at 1700°K. The experimental 1700°K distributions were then fitted to the "expected" distributions as shown in Figs. 11(a)–(d). The position of $V_p=0$ of the "expected" distribution was marked on the V axis of the experimental 1700°K distribution. The shift of the corresponding $V_p=0$ position for the 2000°K distribution is shown at the bottom of Figs. 11(a)–(d). A shift to the right indicates that the *experimental* distribution at 1700°K had to be moved to the right to match the prediction from 2000°K, and means that the work function is lower at 1700°K (positive $d\phi/dT$).

The observed changes of work function, with the exception of the (112) direction, are not much larger than the accuracy of fitting which is estimated as ± 0.005 v. A greater temperature difference would have yielded larger changes. However, the present experimental techniques imposed upper and lower bounds upon the filament temperature. It was found that if the filament were held at 2100°K the current of

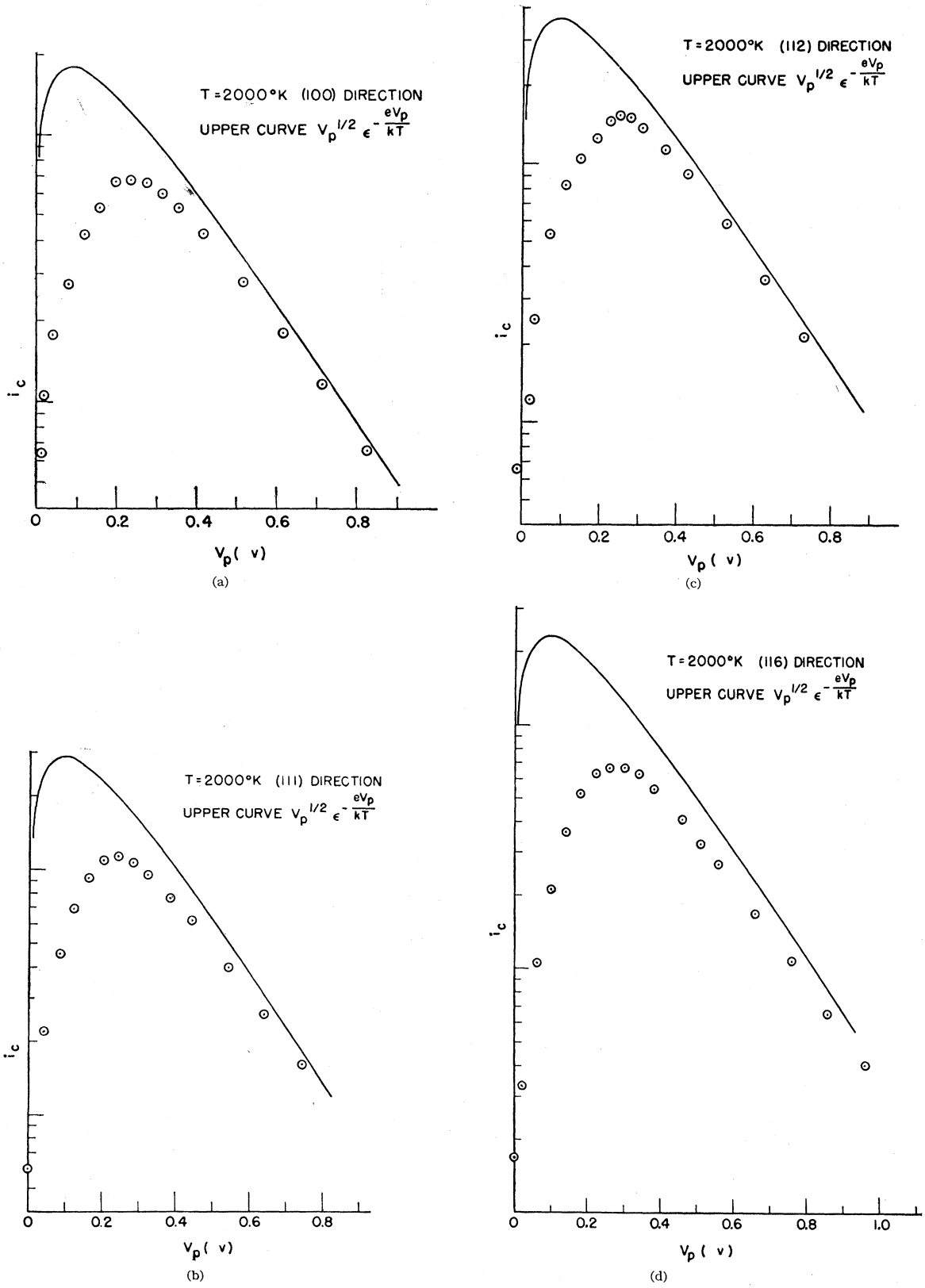

FIG. 10. 2000°K distributions as fitted to the Maxwellian distribution for the determination of experimental $R(V_p)$'s.

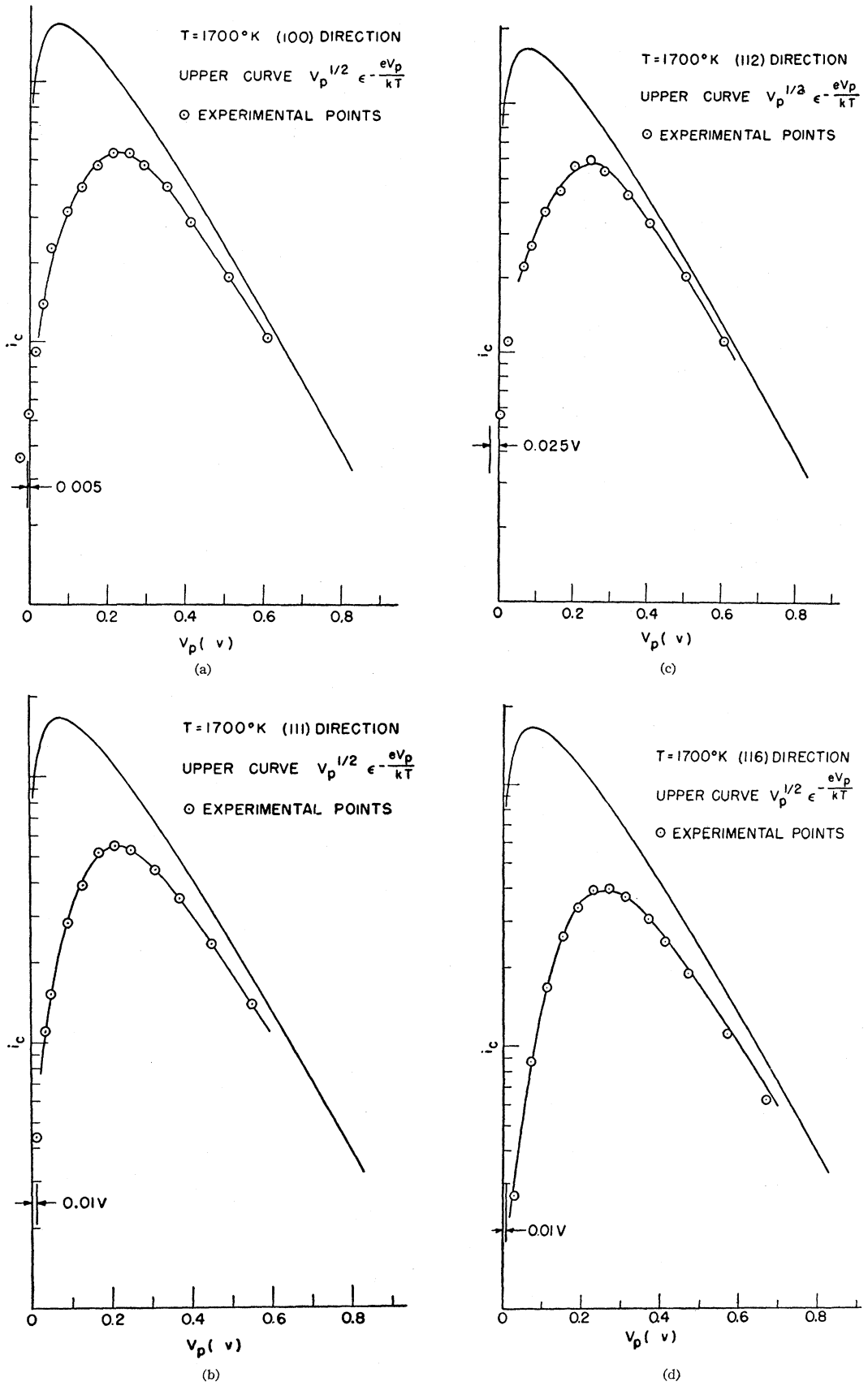

FIG. 11. 1700°K distributions fitted to the distributions expected on the basis of the $R(V_p)$'s observed at 2000°K.

high-energy electrons striking the anode was enough to liberate a perceptible amount of gas. The pressure in the tube as read by the monitoring ionization gauge would rise from 1.5×10^{-9} mm to 4×10^{-9} mm. Under these conditions, the necessary constancy of the analyzer work function could not be guaranteed. No change in the analyzer work function was observed between 2000°K distributions taken before and after a 1700°K distribution.

Temperatures lower than 1700°K did not yield enough collector current for accurate work. Since high resolution was used for these distributions, the fraction of the current finally reaching the collector was quite small, and at 1700°K each point on the energy distribution curve was obtained by the method of "capture of charge." No low-temperature distribution could be taken in the (110) direction. Even at 1800°K the energy distribution in the (110) direction showed distortions in shape due to small, varying leakage currents to the collector, though no shift was observed in comparing it with the distribution taken at 2000°K.

There are two small corrections which should be applied to the observed shifts in V before they can be interpreted in terms of $d\phi/dT$. Both corrections arise from the fact that the applied potential difference between the filament and the analyzer chamber is measured outside the tube. The first is the iR drop, due to the emission current, occurring between the point of measurement of V and the center of the filament, and the second is the thermoelectric emf generated by the temperature difference between these two points.[23] It turned out that the thermoelectric correction cancelled that due to the iR drop to within 10^{-3} v.

The resulting temperature coefficients of the work function of tungsten in the various directions are given in Table II.

Herring and Nichols have summarized the contributions to the temperature derivative of the work function.[24] The sum of the contributions from volume properties such as thermal expansion, internal effects of atomic vibrations upon the electrical and chemical potentials, and the electronic specific heat can be of the order of a few times k/e and of either sign. The magnitudes observed in the present experiment are not inconsistent with this estimate.

VIII. INTERPRETATION OF RICHARDSON PLOT DATA

A summary of the Richardson plot work functions and emission constants published by Nichols[2] and Smith[3] is given in Table III. (The asterisk will be used to distinguish a quantity obtained directly from a Richardson plot.) As Smith pointed out, the data for the (110) direction do not correctly represent the emission in that direction, but rather the sum of the true (110) emission and a spurious current of secondary electrons originating on the inner walls of the anode in the tube used by both Nichols and himself.

[23] Conyers Herring, Phys. Rev. **59**, 889 (1941).
[24] See Table VII on page 244 of reference 1.

TABLE II. Temperature coefficients of work function for crystal faces of tungsten.

Direction	$d\varphi/dT$ (volts/degree)[a]
(100)	-1.7×10^{-5}
(111)	$+3.3$
(112)	-8.3
(116)	$+3.3$
(110)	$<5\times10^{-5}$(?)

[a] Estimated error less than 1.6×10^{-5}.

In the present experiment, secondary electrons from the anode do not have enough energy to reach the analyzer. Nor were any significant currents of reflected primaries observed. Reflected primaries from regions of the anode receiving copious emission from one of the low-work-function directions might be expected to have shown themselves as a spurious energy distribution peak when the crystal was oriented for observation of the (110) emission. However, such reflected primaries would be defocused by the lens since their trajectories would not be radial at the anode slit.

In connection with the data in Table III, Smith also points out that his work functions are slightly lower than those obtained originally by Nichols because of the elimination of a small spurious current of photoelectrons leaving the collector. He ascribed the larger discrepancy in measured work functions in the (116) direction to the violent heat treatment given to his crystal in which its diameter decreased 4 percent through evaporation, and "plateaus" developed on the surface of the crystal normal to the (110), (112), and (100) directions.

The crystal used in the present experiment had only mild heat treatment, similar to that given Nichols' original crystal. Therefore, Nichols' original Richardson plot constants in the (116) direction should probably be used for purposes of comparison.

The nonideality of the energy distribution of the thermionic current may be represented by a transmission coefficient $\alpha[1-R(V_p)]$. In this expression, $R(V_p)$ is the reflection coefficient obtained from fitting the experimental distribution to the ideal distribution, and α is a constant, less than or equal to unity, which can take account of a reflection which varies so slowly with energy that it cannot be detected in the fitting

TABLE III. Summary of Richardson-plot work functions and emission constants.

Direction	Nichols φ^*	Nichols A^*	Smith φ^*	Smith A^*
(111)	4.39	35	4.38	52
(112)	4.69	125	4.65	120
(116)	4.39	53	4.29	40
(100)	4.56	117	4.52	105
(110)	4.68	15	4.58	8

TABLE IV. Compatibility of the data on differences between true work functions, temperature variations of true work functions, and differences between Richardson-plot work functions.

Direction "a"	$(\varphi_a-\varphi_{111})$	$(\varphi_a{}^*-\varphi_{111}{}^*)$	$\frac{(\varphi_a-\varphi_{111})-(\varphi_a{}^*-\varphi_{111}{}^*)}{T}$	$\left(\frac{d\varphi_a}{dT}-\frac{d\varphi_{111}}{dT}\right)$ [a]
(116)	−0.01	0 [b]	-0.5×10^{-5}	0
(100)	+0.02	+0.14	-6.0×10^{-5}	-5.0×10^{-5}
(112)	+0.12	+0.27	-7.5×10^{-5}	-11.6×10^{-5}
(110)	+0.71	?	?	?

[a] The error in the observed differences may be as large as 3×10^{-5} v deg^{-1}. See Table II.
[b] The old Nichols values of $\varphi_{116}{}^*=\varphi_{111}{}^*=4.39$ v were used.

process. Richardson's equation for the saturation emission current density may then be written as

$$j=\alpha A(1-\bar{R})T^2\exp(-e\varphi/kT), \tag{4}$$

where $\bar{R}$ is the average of $R(V_p)$ over the Maxwellian distribution. The quantities derived from a Richardson plot are then[25]

$$\varphi^*=\varphi-T\frac{d\varphi}{dT}-\frac{kT^2}{e(1-\bar{R})}\frac{d\bar{R}}{dT}, \tag{5}$$

$$A^*=\alpha A(1-\bar{R})\exp\left[-\frac{e}{k}\frac{d\varphi}{dT}-\frac{T}{(1-\bar{R})}\frac{d\bar{R}}{dT}\right]. \tag{6}$$

A check on the self-consistency of the present data on work-function differences and $d\phi/dT$, and the Nichols-Smith values of ϕ^* can be made. From the direct comparison of the energy distributions (Fig. 5) it can be inferred that $\bar{R}$ and $d\bar{R}/dT$ are very much the same for all of the surfaces. Therefore, if Eq. (5) is considered for two surfaces, "a" and "b," we may write

$$\frac{(\varphi_a-\varphi_b)-(\varphi_a{}^*-\varphi_b{}^*)}{T}=\left(\frac{d\varphi_a}{dT}-\frac{d\varphi_b}{dT}\right). \tag{7}$$

The compatibility of the data in terms of Eq. (7) at 2000°K is shown in Table IV. The only discrepancy is in the (112) direction. The assumption that the term involving $\bar{R}$ in Eq. (5) cancels out in taking the differences between the (112) and (111) directions was found to be satisfactory by numerical integration of the experimental $R(V_p)$'s for these directions. It is felt that the contact potential measurements between the surfaces are sufficiently accurate to rule out an error in $(\phi_{112}-\phi_{111})$ which could cause the discrepancy. The remaining possibilities are that the negative temperature coefficient of the (112) work function is not as large as the present measurements indicate or that $\phi_{112}{}^*$ is about 0.09 v too low.

It is interesting to compute the quantity $A\alpha$ from Eq. (6) using the measured values of $d\phi/dT$, the Nichols-Smith A^*'s, and Nottingham's reflection coefficient for $\bar{R}$ and $d\bar{R}/dT$. The Nottingham reflection coefficient is a good representation of the observed reflection, and integrates to the simple form $\bar{R}=(1+kT/\omega)^{-1}$. Table V shows the calculated values of $A\alpha$ for the different directions. For the (100), (111), and (116) directions, the values are the same to within the experimental uncertainties of 10 percent in A^* and 20 percent in $\exp[(e/k)(d\phi/dT)]$. A reasonable value of $\alpha=0.9$ seems to be indicated. The discrepancy appearing here in the (112) direction is of the same nature as that found in Table IV. In fact, if the temperature coefficient in the (112) direction is assumed to be -4.2×10^{-5} v/deg instead of the -8.3×10^{-5} v/deg which was measured, the discrepancy is completely removed from both tables. However, if the measured temperature coefficient in the (112) direction is presumed correct, then it must be assumed that the Richardson plot measurement of $\phi_{112}{}^*$ is low by roughly 0.08 v and that $A_{112}{}^*$ should have been about 190. This sort of error in the Richardson plot values could

TABLE V. Emission constants $A\alpha$(amperes/cm^3 deg^2) obtained by correcting the Richardson-plot A^* values for the observed temperature variation of the work functions and the non-Maxwellian character of the energy distributions.

Direction	A^*	$A\alpha$
(111)	52	101
(112)	120	61
(116)	53[a]	103
(100)	105	113

[a] The old Nichols value.

[25] See Sec. I.5 of reference 1.

TABLE VI. Best estimates of the true work functions for a tungsten crystal in the temperature range 1700°K to 2000°K utilizing measured temperature variations and Nottingham's reflection coefficient.

Direction	φ in volts
(111)	$4.30+(3\times10^{-5})T$
(112)[a]	$4.57-(5\times10^{-5})T$ or $4.66-(8\times10^{-5})T$
(116)[b]	4.20 to $4.31+(3\times10^{-5})T$
(100)	$4.44-(2\times10^{-5})T$
(110)	5.09 at $T=2000°$

[a] The first value corresponds to the assumption that the Richardson plot data were not affected by a spurious current and the second is based upon the observed temperature coefficient.
[b] The spread in work function is assumed to be due to differences in heat treatments of the crystals.

have been due to a small amount of the same type of background current that invalidated the (110) Richardson plots.[3]

Table VI shows the best estimates of true work function for the various directions in the thermionic temperature range obtained from Eq. (5) [and the measured work-function differences for the (110) direction]. It should be pointed out that an extrapolation of the values of Table VI to room temperature would be of doubtful validity since $d\phi/dT$ cannot be expected to remain constant over large ranges of temperature.

Since the experimental Richardson plots cover the temperature range from 1500°K to 2000°K, the effect of reflection was calculated at 1700°K for Tables V and VI. This procedure amounts to finding the slope and intercept of the straight line which would be tangent to the Richardson plot points at 1700°K.

IX. CONCLUDING REMARKS

The energy distributions observed in this experiment have, as yet, no satisfactory theoretical explanation. It would seem extremely unlikely that the various surfaces of a single crystal of tungsten would be patchy in just such a manner as to yield identical energy distributions. The possibility that the observed reflection could be due to the band structure of tungsten seems to be ruled out by the consideration that the emission in the (110) direction must originate at a point 0.7 ev higher in energy than the emission in the (111) direction.

The author would like to express his gratitude to Professor W. B. Nottingham for suggesting this problem and for his advice and encouragement while the research was in progress. He is also grateful to the Radio Corporation of America for the RCA Fellowship in Electronics which he held during part of this work.

PHYSICAL REVIEW VOLUME 98, NUMBER 4 MAY 15, 1955

Density of States Curve for Nickel*

G. F. KOSTER†
Massachusetts Institute of Technology, Cambridge, Massachusetts
(Received December 24, 1954)

A density of states curve for the d bands in nickel is presented. This curve is an extension over the entire energy range of the d bands of the density of states curve for nickel already computed by Fletcher and Wohlfarth. The matrix of the interaction of the d states with the periodic potential is exactly the same as was used by Fletcher and Wohlfarth.

IN a recent paper[1] by Slater and the author, a density of states curve for the d electrons in the body-centered structure was calculated using the tight-binding approximation. In this approximation, the solution for the energies of the periodic potential problem is assumed to consist of linear combinations of Bloch functions made out of atomic orbitals. For the d electrons, the solution is assumed to consist of a linear combination of Bloch sums made out of the five d atomic orbitals. The matrix of the Hamiltonian when formed between these Bloch sums involves parameters which represent the interaction between a d atomic orbital located at the central lattice site in the crystal with d atomic orbitals located at neighboring lattice sites. In the aforementioned paper, the values of these parameters were taken from a paper by Fletcher and Wohlfarth[2] who had calculated the band structure of face-centered nickel. From the band structure obtained in this way a density of states, representing the number of energy levels in a given energy range, was obtained. The striking feature of the density of states curve obtained in this way for the d electrons in the body-centered structure is a pronounced dip at center of the density of states. Since the shape of the density of states curve for the transition metals is important in problems of magnetism and electronic

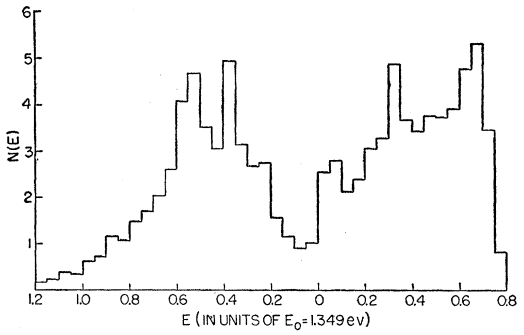

FIG. 1. Density of states $N(E)$ as a function of energy for the d bands in nickel.

* The research in this paper was supported jointly by the Army, Navy, and Air Force under contract with the Massachusetts Institute of Technology.
† Staff Member, Lincoln Laboratory, Massachusetts Institute of Technology, Cambridge, Massachusetts.
[1] J. C. Slater and G. F. Koster, Phys. Rev. **94**, 1498 (1954).
[2] G. C. Fletcher and E. P. Wohlfarth, Phil. Mag. **42**, 106 (1951); G. C. Fletcher, Proc. Phys. Soc. (London) **A65**, 192 (1952).